Magnetodielectric coupling in the ilmenites MTiO_{3} (M=Co, Ni)

Jaye K. Harada, Luke Balhorn, Josef Hazi, Moureen C. Kemei, and Ram Seshadri

Magnetodielectric coupling in the ilmenites MTiO$_3$ (M = Co, Ni)

Jaye K. Harada,[*] Luke Balhorn, Josef Hazi, Moureen C. Kemei, and Ram Seshadri[†]

Materials Department and Materials Research Laboratory,
University of California, Santa Barbara, California 93106
(Dated: February 9, 2016)

We report magnetodielectric coupling in rhombohedral ilmenites CoTiO$_3$ and NiTiO$_3$ along with heat capacity and magnetic measurements. CoTiO$_3$ and NiTiO$_3$ undergo antiferromagnetic ordering at ≈ 38 K and ≈ 22 K respectively. The dielectric permittivity of CoTiO$_3$ decreases below its magnetic ordering temperature while the dielectric permittivity of NiTiO$_3$ increases below the Néel temperature. The dielectric permittivity of CoTiO$_3$ and NiTiO$_3$ are dependent on the applied magnetic field and temperature with the strongest dependence observed close to the magnetic ordering temperature. We analyze magnetodielectric coupling in CoTiO$_3$ and NiTiO$_3$ on the basis of spin-phonon coupling and suggest other possible mechanisms such as exchange coupling and magnetostrictive effects.

I. INTRODUCTION

In the past few decades, magnetoelectrics have experienced a revival in research efforts,[1] in part because of the colossal magnetodielectric effect observed in some materials.[2,3] Enhancement of the magnetodielectric effect could lead to new devices such as tunable filters, magnetic sensors, and spin-charge transducers. However, the search and prediction of new magnetoelectric materials has proved to be challenging. Current efforts address the search for new classes of magnetoelectric materials and the quest for systems exhibiting strong coupling between magnetization and electric polarization.

While early research efforts focused on creating materials to facilitate both magnetism and ferroelectricity, recent literature has shown complex spin structures,[4] magnetostructural,[5] and magnetoelastic[6] coupling can also facilitate magnetodielectric coupling. The discovery of new magnetodielectric materials can further our understanding of these mechanisms and guide us in the direction of a system with strong coupling. Magnetodielectric coupling has been reported in MnTiO$_3$,[7] an ilmenite with the non-polar crystal structure $R\bar{3}$. In this contribution, we investigate the magnetic and dielectric properties of related ilmenites and show that CoTiO$_3$ and NiTiO$_3$ display magnetodielectric coupling. We speculate on the possible mechanisms of magnetodielectric coupling on the basis of spin-phonon coupling.

CoTiO$_3$ (Fig. 1) has a $R\bar{3}$ crystal symmetry and consists of alternate layers of corner sharing CoO$_6$ and TiO$_6$ octahedra, alternately stacked along the c axis. Its magnetic structure has been reported to consist of ferromagnetic sheets of Co^{2+} on the $a - b$ plane which are antiferromagnetically coupled along the c axis. CoTiO$_3$ transitions from a paramagnetic to an antiferromagnetic state at $T_N \approx 38$ K.[8–10] The magnetic moments of CoTiO$_3$ are completely ordered at low temperatures.[8]

We have also examined magnetodielectric coupling in the ilmenite NiTiO$_3$ (Fig. 1), which has the same $R\bar{3}$ crystal structure of CoTiO$_3$; corner sharing NiO$_6$ and TiO$_6$ octahedra forming layers that alternate along the c axis. Studies of the electronic properties of this
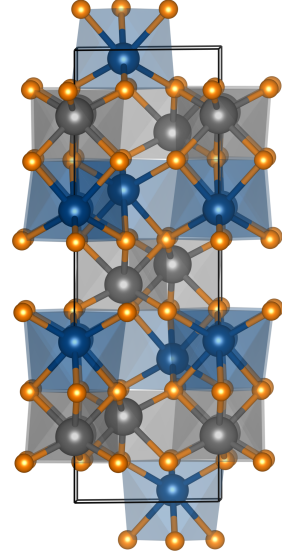

FIG. 1. The ilmenite crystal structure of CoTiO$_3$ and NiTiO$_3$ ($R\bar{3}$) which consists of alternating sheets of corner sharing TiO$_6$ and CoO$_6$/NiO$_6$ octahedra. Ti^{4+} atoms are in the center of in grey/lighter octahedra and and Co^{2+}/Ni^{2+} atoms are in the centers of blue/darker octahedra.

material indicate that it is highly insulating at low temperatures,[11] which makes it a promising candidate for magnetodielectric coupling. Heller *et al.*, found that NiTiO$_3$ is antiferromagnetic below its Néel temperature of ≈ 23 K,[12] and this was corroborated by later studies.[9,10,13] Neutron diffraction studies of the magnetic structure of NiTiO$_3$ by Shirane *et al.* revealed sheets of ferromagnetic Ni^{2+} moments on the $a - b$ plane and antiferromagnetic coupling between these sheets along the c axis,[14] analogous to what is seen in CoTiO$_3$. The spins are oriented perpendicular to the (111) direction and at 4.2 K, NiTiO$_3$ was found to be only 88 % ordered.[14]

Here, we report magnetodielectric coupling in the ilmenites CoTiO$_3$ and NiTiO$_3$. We show that magnetic ordering occurs concurrently with changes in the dielectric permittivity. Isothermal magnetic field-dependent

measurements of the dielectric permittivity show a small enhancement of the magnetocapacitance near the magnetic ordering temperatures.

II. METHODS

Polycrystalline $CoTiO_3$ and $NiTiO_3$ were prepared from stoichiometric precursors TiO_2 (>99%, Sigma Aldrich), $CoC_2O_4 \cdot H_2O$, and $NiC_2O_4 \cdot H_2O$. The oxalates were prepared by precipitation from stoichiometric solutions of $Co(C_2H_3O_2)_2 \cdot (H_2O)_4$ (>98%, Alfa Aesar), $Ni(C_2H_3O_2)_2 \cdot (H_2O)_4$, and oxalic acid (>99.5%, Sigma Aldrich). The powders were ground, pressed into pellets, and decomposed in air at $850\,°C$ for $6\,h$, then cooled slowly to room temperature. The powders were then reground, pressed into pellets, sintered at $1100\,°C$ for $48\,h$ followed by quenching in water.

Sample purity and crystal structure was confirmed using high-resolution synchotron X-ray diffraction at the 11BM beamline of the Advanced Photon Source, Argonne National Laboratory. The diffraction data was taken at $295\,K$ using a wavelength of $\lambda = 0.459004\,\text{Å}$. Rietveld refinements were performed using the TOPAS software suite.[15]

Heat capacity measurements were taken with a Quantum Design (QD) physical properties measurement system (PPMS). Magnetic transitions were studied using a QD MPMS XL5 superconducting quantum interference device (SQUID). Field-cooled measurements were taken under a magnetic field of $1\,kOe$. Samples for magnetodielectric measurements were prepared by spark plasma sintering (SPS) of powder samples at $850\,°C$ under a load of $5\,kN$ for $3\,minutes$. SPS takes place under reducing conditions, so sintered pellets were annealed in air at $1100\,°C$ for $12\,h$ and quenched in water to restore their oxygen content. After annealing, samples were characterized using a Phillips X'PERT X-ray diffractometer to confirm no compositional changes took place during densification. To confirm densification of samples, density measurements were performed using a Micromeritics AccuPync 1340 Pyncnometer. The final pellets had a cylindrical shape: $NiTiO_3$ had dimensions of approximately $9.45\,mm$ in diameter and $2.76\,mm$ in height. $CoTiO_3$ had dimensions of approximately $8.95\,mm$ in diameter and $2.87\,mm$ in height. Both sides of the pellet were coated with conducting epoxy to enable electrical measurements. The sample was then clamped on a sample rod to prevent movement due to magnetic fields and then placed in a QD Dynacool PPMS, which was used in combination with an Andeen-Hagerling 2700A capacitance bridge for magnetodielectric measurements. The sample was placed as close to the bottom of the chamber as possible to ensure accurate temperature readings. The capacitance was measured at 1, 2, 5, 10, and $20\,kHz$ with only the $1\,kHz$ data being presented and analyzed in this contribution. The transition temperature in the dielectric measurements was frequency independent in keeping
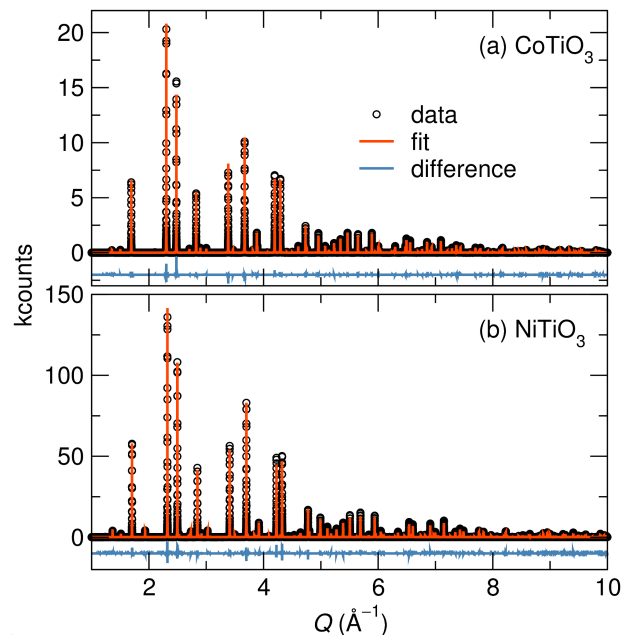

FIG. 2. High-resolution synchrotron powder x-ray diffraction data of (a) $NiTiO_3$ and (b) $CoTiO_3$ measured at $T=295\,K$ and modeled using the $R\overline{3}$ crystal structure. Rietveld analysis revealed that the $NiTiO_3$ sample is $97.0(1)\,wt.\%$ $NiTiO_3$ and $3.0(1)\,wt.\%$ TiO_2, while the $CoTiO_3$ sample is phase pure.

with the highly insulating nature of $CoTiO_3$ and $NiTiO_3$.

III. RESULTS AND DISCUSSION

Rietveld refinement of synchrotron x-ray powder diffraction data shows that both compounds are rhombohedral in the crystal structure $R\overline{3}$ [Fig. 2(a) and (b)]. Refinement of the $CoTiO_3$ diffraction pattern [Fig. 2(b)] shows a phase pure compound with lattice parameters $a = 5.06735(2)\,\text{Å}$ and $c = 13.92213(8)\,\text{Å}$, which are in good agreement with reported structural parameters of this material.[16] Density measurements of powder samples show that $CoTiO_3$ has a density of $4.900(7)\,g/cm^3$ (98.1 % of its theoretical density) and $NiTiO_3$ has a density of $4.930(2)\,g/cm^3$ (97.4 % of its theoretical density). Refinement of the diffraction pattern of $NiTiO_3$ measured at room temperature indicates that the powder is $97.0(1)\,wt.\%$ $NiTiO_3$ and $3.0(1)\,wt.\%$ rutile TiO_2 [Fig. 2(a)]. Ti^{4+} has no unpaired spins and we expect that this impurity has no effect on the magnetic properties of the sample $NiTiO_3$ studied here. $NiTiO_3$ has lattice parameters $a = 5.03140(8)\,\text{Å}$ and $c = 13.7918(2)\,\text{Å}$, which agree with the values reported in literature.[17] The close agreement of the measured densities to the theoretical density also shows that these materials are nearly phase pure, and well-ordered.
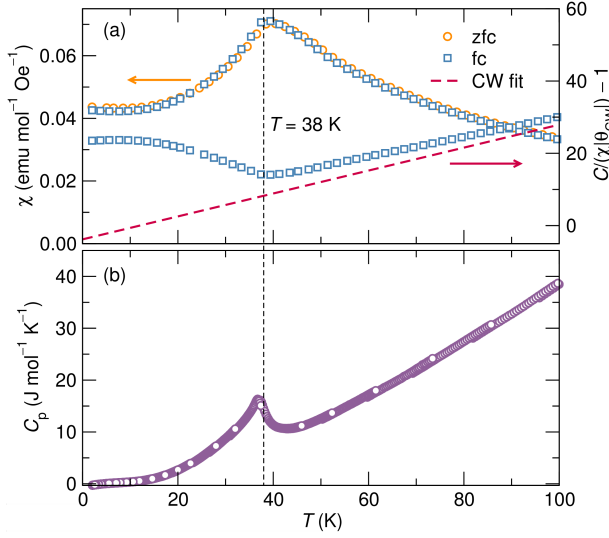
FIG. 3. (a) ZFC and FC magnetic susceptibility measurements of CoTiO$_3$ reveal the onset of antiferromagnetic order around 38 K. Curie-Weiss analysis of the data reveals significant deviation from the paramagnetic model even at high temperatures, suggesting that Curie-Weiss analysis may be inappropriate for this compound. Nevertheless, the extracted Curie-Weiss temperature is 11.94 K and the effective magnetic moment is 5.02 μ_B. (b) Temperature-dependent heat capacity measurements of CoTiO$_3$ show a peak at ≈ 38 K.

A. Magnetic and magnetodielectric properties of CoTiO$_3$

CoTiO$_3$ exhibits magnetic and dielectric phase transitions around 38 K. Antiferromagnetic ordering at $\approx$38 K is evidenced by the peak in the zero-field-cooled (ZFC) and field-cooled (FC) magnetic susceptibility [Fig. 3(a)]. The magnetic transition is concurrent with an anomaly in the heat capacity [Fig. 5(b)]. The inverse of the susceptibility data shows significant deviation from the paramagnetic model even at high temperatures. This suggests that Curie-Weiss analysis of the paramagnetic region is not appropriate, as the Curie-Weiss law only applies if χ has no temperature-dependent contribution from energy levels above the ground state.[18] Nevertheless, Curie-Weiss analysis of the field-cooled magnetic susceptibility data of CoTiO$_3$ in the paramagnetic region $(250\,\text{K} < T < 380\,\text{K})$ gives a Curie temperature of $\theta_{CW} = 12$ K and a effective magnetic moment of $\mu_{eff} = 5.02\,\mu_B$. The positive Curie temperature is inconsistent with the antiferromagnetic ordering found in CoTiO$_3$, but this phenomena has been seen in other systems with Co^{2+} in an octahedral environment, such as GeCo$_2$O$_4$.[18] Additionally, calculations by Goodenough and Stickler[19] predict the Curie-Weiss temperature of this material to be positive due to crystal field splitting. However, this result disagrees with other reports where the Curie temperature was found to be negative.[10,13]
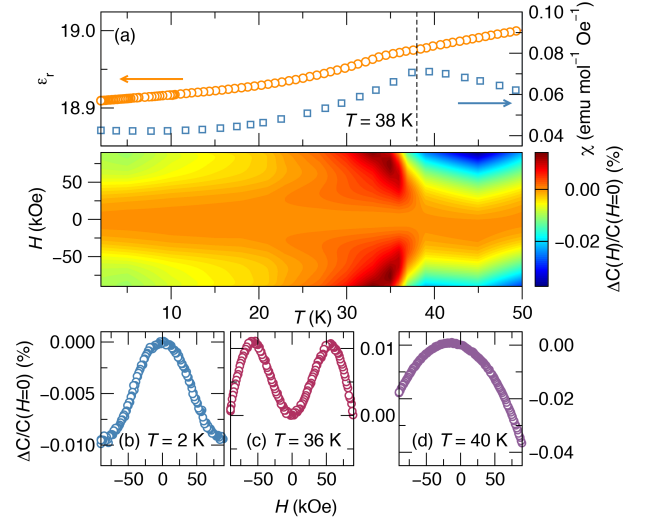
Fig. 4(a) shows the temperature-dependent dielectric

FIG. 4. Magnetodielectric measurements of CoTiO$_3$. (a) Zero-field temperature-dependent dielectric permittivity data and the field-cooled magnetic susceptibility. The dashed line is the Barrett function fit to the dielectric data. The transition in the dielectric permittivity (≈ 33 K) occurs at a slightly lower temperature than the magnetic transition. The contour plot was generated from isothermal field-dependent dielectric permittivity measurements, details on the generation of this plot can be found in the text. The intensity is the percent change in capacitance from the zero-field value, or the magnetocapacitance. The isothermal field-dependent magnetocapacitance measurements at (b) 2 K, (c) 36 K, and (d) 40 K show trends in the field dependence at various temperature regimes.

data under zero applied magnetic field. There is a gradual decrease in the dielectric permittivity with decreasing temperature until about 33 K, where there is a abrupt decrease in the dielectric permittivity. This transition occurs at a significantly lower position than the magnetic transition. To relate the dielectric permittivity to relevant transverse optical (TO)-phonon modes, we have followed the analysis of studies on MnO[20] and MnF$_2$.[21] We used the Barrett function to fit the temperature-dependent dielectric data:

$$\epsilon(T) = \epsilon(0) + A/[\exp(h\nu_t/k_B T) - 1] \qquad (1)$$

Where A is the coupling constant, h is the Planck constant, ν_t is the mean frequency of the final states in the lowest lying optical-phonon branch, and k_B is the Boltzmann constant. The Barrett function was fit in the temperature range $40\,\text{K} < T < 85\,\text{K}$. The refined parameters of the fit are $\epsilon(0) = 18.96$, $A = 0.215$, and $\nu_t = 61$ cm^{-1}.

We have also examined trends in the isothermal dielectric permittivity as a function of a varying magnetic field. The contour plot of dielectric permittivity data in Fig. 4 was generated from many isothermal magnetic field-dependent dielectric measurements. The isothermal magnetic field-dependent data was interpolated as a function of applied magnetic field using a tenth order

polynomial, then interpolated again as a function of temperature from 2 K to 50 K. The intensity of the contour plot is the percent change in capacitance normalized to the $H = 0$ value, which we will refer to as the magnetocapacitance. Figs 4(a) and 4(b) are provided to help visualize the isothermal field-dependent magnetocapacitance at different regimes.

Magnetic field-dependent dielectric permittivity data in CoTiO3 shows three different regimes of trends in the magnetic field-dependent data. Between 2 K and 24 K, dielectric permittivity decreases with increasing magnetic field. Between 24 K and 36 K, local maxima in field-dependent magnetocapacitance are observed at intermediate magnetic fields. Above the transition temperature at 36 K, dielectric permittivity decreases with increasing magnetic field according to a quadratic relationship. The magnitude of the magnetocapacitance is largest near the transition temperature, which is unusual. Typically magnetocapacitance is enhanced as the temperature decreases, but we observe the opposite trend here.

To ensure that magnetodielectric coupling in these ilmenites is not due to Maxwell-Wagner effects,[22] we measured the dielectric loss ($\tan \delta$) concurrently with all measurements and concluded that the data shown are all intrinsic. The dielectric loss of CoTiO$_3$ were very small ($\tan \delta < 0.00002$) and though we saw some dependence of the dielectric loss on the applied magnetic field when measured below 10 K, it was inconsistent with extrinsic effects due to the electrode-sample interface.

B. Magnetic and magnetodielectric properties of NiTiO$_3$

NiTiO$_3$ undergoes an antiferromagnetic transition at a lower temperature than CoTiO$_3$. A peak is observed around 22 K in the ZFC and FC magnetic susceptibility [Fig. 5(a)]. The observed Néel temperature of NiTiO$_3$ is consistent with reported values in the literature.[9,10,12,13] The positive divergence of the inverse scaled susceptibility from the paramagnetic mode is indicative of compensated antiferromagnetic interactions. Curie-Weiss analysis of the field-cooled magnetic susceptibility from $250\,\mathrm{K} < T < 380\,\mathrm{K}$ gives a Curie temperature of $\theta_{CW} = -14\,\mathrm{K}$, which agrees with some of the θ_{CW} values in the literature ($\theta_{CW} = -13\,\mathrm{K},$[10] $-55\,\mathrm{K},$[13] $-58\,\mathrm{K}$[9]). The effective magnetic moment (μ_{eff}) derived from Curie-Weiss analysis is $\mu_{\mathrm{eff}} = 3.21\,\mu_B$. This moment is slightly higher than the calculated effective moment of Ni^{2+} ion in octahedral environments, computed to be $\mu_{\mathrm{eff}} = 2.83\,\mu_B$, likely suggesting a small orbital contribution to the magnetism of NiTiO$_3$. Our extracted $\mu_{\mathrm{eff}} = 3.21\,\mu_B$ is consistent with several reports that describe slightly increased effective magnetic moments in this compound.[9,10,13] Heat capacity measurements show a peak at the magnetic ordering temperature indicating a change in the entropy as NiTiO$_3$ transitions from a paramagnetic to an antiferromagnetic state [Fig. 5(b)].
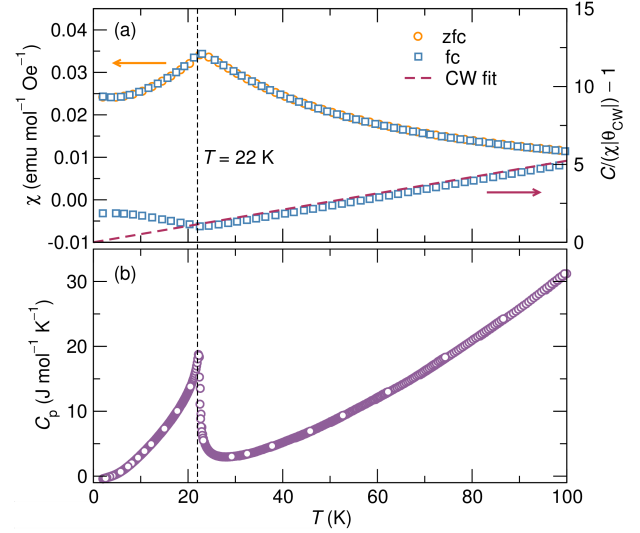

FIG. 5. (a) Zero-field-cooled and field-cooled magnetic susceptibility measurements and Curie-Weiss analysis of NiTiO$_3$. The peak in the ZFC and FC measurements reveals the onset of antiferromagnetic order. Curie-Weiss analysis of the FC data gives a Curie-Weiss temperature of $-14\,\mathrm{K}$ and a magnetic moment of $3.21\,\mu_B$. (b) The temperature-dependent heat capacity of NiTiO$_3$ shows a peak at $22\,\mathrm{K}$.

Temperature-dependent dielectric measurements of NiTiO$_3$ at zero-field show an anomaly in the dielectric permittivity at approximately 22 K where a magnetic phase transition occurs [Fig. 6(a)]. A significant increase in the dielectric permittivity occurs below 22 K [Fig. 6(a)]. This is in contrast to CoTiO$_3$ where a decrease in dielectric permittivity is seen below T$_N$. This difference in trends may be solved with dielectric measurements of single crystal samples, as other materials, such as MnO and MnF$_2$, have shown positive and negative trends in dielectric permittivity along different axes.[20,21]

The Barrett function (Eq. 1) was again fit to the temperature-dependent dielectric data from $25\,\mathrm{K} < T < 85\,\mathrm{K}$. The refined parameters are $\epsilon(0) = 14.83$, $A = 0.280$, and $\nu_t = 288\,\mathrm{cm}^{-1}$. Raman spectroscopy on polycrystalline NiTiO$_3$ shows a peak at $284\,\mathrm{cm}^{-1}$,[23] though it has not been assigned to an optical or electronic mode.

A contour plot of the NiTiO$_3$ magnetocapacitance data (contour plot in Fig. 6) was created using the same methods as the CoTiO$_3$ contour plot. Below T_N, the magnetocapacitance decreases with increasing field and constant temperature. Above T_N, it increases with increasing field and the magnitude of the magnetocapacitance decreases with increasing temperature. This plot shows a strong dependence of the isothermal dielectric permittivity on the applied field very close to the magnetic ordering temperature, as is indicated by the large contrast near T_N. Like CoTiO$_3$, NiTiO$_3$ also exhibits a strong dependence of the dielectric permittivity on the applied field near T_N.
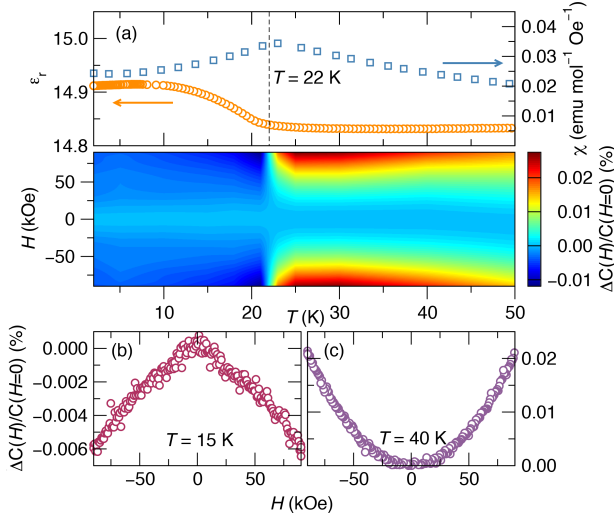
The dielectric loss of NiTiO$_3$ samples was also mea-

FIG. 6. Magnetodielectric measurements of NiTiO$_3$. (a) Zero-field, temperature-dependent dielectric permittivity measurements of NiTiO$_3$ plotted alongside the field-cooled magnetic susceptibility. The dashed line is the Barrett function fit to the dielectric data. The transition in the dielectric permittivity is concurrent with the magnetic transition. The contour plot was generated from isothermal field-dependent dielectric permittivity measurements, details can be found in the text. The intensity of the contour plot is the percent change in capacitance from the zero-field value, or the magnetocapacitance. The isothermal field-dependent magnetocapacitance measurements at (b) 15 K and (c) 40 K are provided to show more details in the different regimes of magnetocapacitance.

sured concurrently with all dielectric measurements to ensure all effects seen are intrinsic to the material. The dielectric loss in all measurements were flat (i.e. independent of temperature and applied field) and small, indicating no extrinsic effects.

IV. DISCUSSION

Exchange striction, the movement of interacting magnetic cations to strengthen magnetic interactions, is thought to be the mechanism behind magnetodielectric coupling in Y$_2$Cu$_2$O$_5$[24] and the spinel NiCr$_2$O$_4$.[25]. As a result, magnetic ordering in these spinels occurs concomitantly with structural distortions. NiCr$_2$O$_4$ also exhibits magnetodielectric coupling, which Sparks *et al.* have described as a sensitive probe for magnetostructural coupling.[5] This proposition leads to the hypothesis that CoTiO$_3$ and NiTiO$_3$ likely undergo magnetostriction at the onset of antiferromagnetic order. High resolution x-ray powder diffraction studies at low temperature would shed light on this. This suggestion is further strengthened by magnetostrictive effects measured in the related ilmenite FeTiO$_3$[26] and the quadratic field-dependent dielectric behavior observed here.

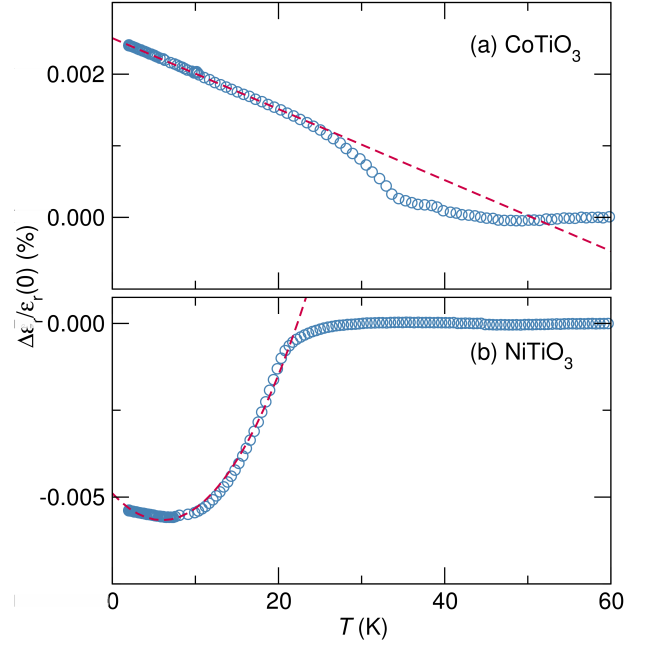A remarkable feature of the magnetocapacitance

FIG. 7. Normalized difference between the dielectric fitting parameter from the Barrett fit, $\epsilon(0)$, and dielectric data for (a) CoTiO$_3$ and (b) NiTiO$_3$. The dashed line is a (a) linear and (b) quadratic fit of the data below T$_N$.

of CoTiO$_3$ and NiTiO$_3$ is the strong dependence of the capacitance on the applied field near the magnetic ordering temperature. The trends measured in CoTiO$_3$ and NiTiO$_3$ are reminiscent of magnetodielectric measurements of CuFe$_{0.95}$Rh$_{0.05}$O$_2$,[27] FeVO$_4$,[28] and YBaCuFeO$_5$[29] in that they all show an increase in the magnitude of field-dependent magnetocapacitance just below T_N. Two of these also show a significant drop off in the magnetocapacitance just above T_N,[27,28] which is seen here. They attribute these trends to a transition from a non-polar to a polar structure, which has not been seen in the ilmenites. They also note that there are likely competing factors that are contributing to the magnetodielectric behavior, such as spin-reorientation and anomalies in magnetostriction.

Other possible mechanisms for magnetodielectric coupling below the transition temperature include a magnetic contribution. The relationship between magnetization and the dielectric permittivity can be modeled using Ginzburg-Landau theory which describes the free energy of the system, F, in terms of polarization P, and the magnetization M:

$$F = \frac{1}{2\epsilon_0}P^2 - PE - \alpha PM + \beta PM^2 + \gamma P^2 M^2 + \mathcal{O}(n) \quad (2)$$

Here α, β, and γ are magnetoelectric coupling coefficients. The dielectric is defined as the second derivative of F in terms of P. Solving for the dielectric $\frac{\partial^2 F}{\partial P^2} = \epsilon \propto \gamma M^2$ or γL^2, where L is the sublattice magnetization. Because CoTiO$_3$ and NiTiO$_3$ are antiferromag-

netic, we use L in place of M. We note that this mechanism is unlikely, as the temperature- and field-dependent dielectric do not fit a quadratic curve. This is difficult to see in the temperature-dependent case, so we have subtracted the dielectric fitting parameter from the Barrett fit, $\epsilon(0)$, from the experimental data and normalized by the same value it to obtain $\frac{\Delta\epsilon_r}{\epsilon_r(0)}$ as seen in Fig. 7. The trend in $CoTiO_3$ is obviously linear, while $NiTiO_3$ is not well fit to a quadratic function.

V.   CONCLUSIONS

In summary, we report the preparation and characterization of the magnetic, heat capacity, and magnetodielectric properties of $CoTiO_3$ and $NiTiO_3$. We show that the antiferromagnetic transitions of these ilmenites are accompanied by changes in the dielectric permittivity. We have also demonstrated the magnetic field dependence of the dielectric permittivity of these materials below the Néel temperature. We show the enhanced response of the dielectric permittivity to an applied magnetic field near the Néel temperature. Magnetodielectric coupling in $CoTiO_3$ and $NiTiO_3$ may be due to spin-phonon coupling and magnetostrictive effects. Further studies of the magnetic and nuclear structures of these materials in the antiferromagnetic phase could reveal insights into the origin of the magnetodielectric coupling.

[*] jkharada@mrl.ucsb.edu
[†] seshadri@mrl.ucsb.edu
[1] M. Fiebig, J. Phys. D **38**, R123 (2005).
[2] N. Hur, S. Park, P. A. Sharma, S. Guha, and S.-W. Cheong, Phys. Rev. Lett. **93**, 107207 (2004).
[3] B. Lorenz, Y. Q. Wang, Y. Y. Sun, and C. W. Chu, Phys. Rev. B **70**, 212412 (2004).
[4] M. C. Kemei, S. L. Moffitt, L. E. Darago, R. Seshadri, M. R. Suchomel, D. P. Shoemaker, K. Page, and J. Siewenie, Phys. Rev. B **89**, 174410 (2014).
[5] T. D. Sparks, M. C. Kemei, P. T. Barton, R. Seshadri, E.-D. Mun, and V. S. Zapf, Phys. Rev. B **89**, 024405 (2014).
[6] U. Adem, L. Wang, D. Fausti, W. Schottenhamel, P. H. M. van Loosdrecht, A. Vasiliev, L. N. Bezmaternykh, B. Büchner, C. Hess, and R. Klingeler, Phys. Rev. B **82**, 064406 (2010).
[7] N. Mufti, G. R. Blake, M. Mostovoy, S. Riyadi, A. A. Nugroho, and T. T. M. Palstra, Phys. Rev. B **83**, 104416 (2011).
[8] R. E. Newnham, J. H. Fang, and R. P. Santoro, Acta Crystallogr. **17**, 240 (1964).
[9] H. Watanabe, H. Yamauchi, and H. Takei, J. Magn. Magn. Mater. **1518, Part 2**, 549 (1980).
[10] J. Stickler, S. Kern, A. Wold, and G. Heller, Phys. Rev. **164**, 765 (1967).
[11] Y. Ishikawa and S. Sawada, J. Phys. Soc. Jpn. **11**, 496 (1956).
[12] G. S. Heller, J. J. Stickler, S. Kern, and A. Wold, J. Appl. Phys. **34**, 1033 (1963).
[13] Y. Ishikawa and S. iti Akimoto, J. Phys. Soc. Jpn. **13**, 1110 (1958).
[14] G. Shirane, S. J. Pickart, and Y. Ishikawa, J. Phys. Soc. Jpn. **14**, 1352 (1959).
[15] A. A. Coelho, "Topas academic, v4.1," computer software (2007).
[16] K. Kidoh, K. Tanaka, F. Marumo, and H. Takei, Acta Crystallog. Sect. B **40**, 92 (1984).
[17] M. Ohgaki, K. Tanaka, F. Marumo, and H. Takei, Mineral. J. **14**, 133 (1988).
[18] P. T. Barton, M. C. Kemei, M. W. Gaultois, S. L. Moffitt, L. E. Darago, R. Seshadri, M. R. Suchomel, and B. C. Melot, Phys. Rev. B **90**, 064105 (2014).
[19] J. B. Goodenough and J. J. Stickler, Phys. Rev. **164**, 768 (1967).
[20] M. S. Seehra and R. E. Helmick, Phys. Rev. B **24**, 5098 (1981).
[21] M. S. Seehra and R. E. Helmick, J. Appl. Phys. **55** (1984).
[22] G. Catalan, Appl. Phys. Lett. **88**, 102902 (2006).
[23] M. Baraton, G. Busca, M. Prieto, G. Ricchiardi, and V. Escribano, J. Solid State Chem. **112**, 9 (1994).
[24] U. Adem, G. Nnert, Arramel, N. Mufti, G. R. Blake, and T. T. Palstra, Eur. Phys. J. B **71**, 393 (2009).
[25] M. R. Suchomel, D. P. Shoemaker, L. Ribaud, M. C. Kemei, and R. Seshadri, Phys. Rev. B **86**, 054406 (2012).
[26] M. Charilaou, D. Sheptyakov, J. F. Löffler, and A. U. Gehring, Phys. Rev. B **86**, 024439 (2012).
[27] B. Kundys, A. Maignan, D. Pelloquin, and C. Simon, Solid State Sci. **11**, 1035 (2009), e-MRS symposium N and R.
[28] M. Frontzek, J. T. Haraldsen, A. Podlesnyak, M. Matsuda, A. D. Christianson, R. S. Fishman, A. S. Sefat, Y. Qiu, J. R. D. Copley, S. Barilo, S. V. Shiryaev, and G. Ehlers, Phys. Rev. B **84**, 094448 (2011).
[29] B. Kundys, A. Maignan, and C. Simon, Appl. Phys. Lett. **94**, 072506 (2009).